Original paper

Folia Neuropathologica

Effects of ischemia-hypoperfusion on neuro-vascular units in dual transgenic mice with Alzheimer's disease

Linjuan Sun[1], Chengfu Li[2], Jiangang Liu[1], Nannan Li[1], Fuhua Han[3], Dandan Qiao[1], Zhuang Tao[4], Min Zhan[1], Wenjie Chen[1], Yunling Zhang[1], Xiaoying Zheng[5]

[1]Department of Neurology, Xiyuan Hospital, China Academy of Chinese Medical Sciences, Beijing, P.R. China, [2]China Population and Development Research Center, Beijing, P.R. China, [3]Beijing University of Chinese Medicine, Beijing, P.R. China, [4]China Academy of Chinese Medical Sciences, Beijing, P.R. China, [5]Department of Institute of Population Research, Peking University, Beijing, P.R. China

Folia Neuropathol 2022; 60 (2): 237-249 *DOI: https://doi.org/10.5114/fn.2022.117278*

Abstract

Introduction: *The study aimed to investigate the effects of ischemia on neuro-vascular units in transgenic mice, and to investigate the role of ischemia-hypoperfusion in the model of dual transgenic mice with dementia.*

Material and methods: *In this study, the ischemic model was generated by operating a bilateral common carotid artery micro-embolism. Mice were divided into four groups, including group 1: C57BL sham surgery group (control), group 2: C57BL ischemic group, group 3: amyloid precursor protein/presenilin-1 (APP/PS1) group, and group 4: APP/PS1 ischemic group. Each group comprised 20 mice. Spatial behavior and memory ability of mice were detected by Morris water maze and jumping platform test. Mouse hippocampus was observed by HE staining and Congo red staining. Ultrastructure of each group of neuro-cyclic units was observed by electron microscopy. Various biochemical indicators were detected by ELISA. Western blot detected the amount of protein expression. qRT-PCR identified mRNA expression.*

Results: *The results indicated that learning and memory functions of C57 ischemic mice were lower than those of control group. Positive expression area of APP in APP/PS1 ischemic group was higher than in APP/PS1 group. In APP/PS1 group and APP/PS1 ischemic group, the content of Aβ was significantly higher than in C57 ischemic group. Electron microscopic observation revealed that there were more mitochondrial vacuoles in hippocampal neurons of APP/PS1 mice, and the structure was relatively intact. Mitochondrial vacuoles in hippocampus increased significantly, and vascular wall proliferated in APP/PS1 ischemic group. Compared with C57 control group, the content of vascular endothelial growth factor (VEGF) increased significantly in C57 ischemic group.*

Conclusions: *Ischemia deteriorates the learning and memory function of transgenic mice, aggravates the damage of neuro-vascular units, and impairs the blood–brain barrier transport of Aβ, leading to an increase in the concentration of Aβ cerebrospinal fluid, and further deterioration of neuro-vascular units. At the same time, ischemia is an effective stimulating factor in the release of VEGF.*

Key words: *hypoperfusion, Alzheimer's disease, transgenic mice, neuro-vascular unit, ischemia-hypoperfusion.*

Introduction

Alzheimer's disease (AD) is one of the most common neuro-degenerative diseases, and accounts for more than 80% of patients with dementia [1,4,39]. The age-adjusted prevalence of dementia is above 6.9% in Northern China (4.2% with AD) and 3.9% in Southern China, and 2.8% of people over 65 years

Communicating author:
Xiaoying Zheng, Department of Institute of Population Research, Peking University, 5 Yiheyuan Road, Haidian District, Beijing 100087, China, phone: +86-13621224975, e-mail: zhengxiaoying_kr@163.com

old have AD. Clinical features of AD include disorders involving memory, comprehension, speech, judgment, calculation, and movement, all of which may be accompanied by hallucinations, delusions, behavioral disorders, and personality changes [12-15,35]. The pathogenesis of AD includes Aβ cascade reaction theory, Tau protein hyperphosphorylation theory, neuro-inflammation theory, oxidative stress theory, and neuro-vascular unit theory [3,10,11,42]. Among them, neuro-vascular units play a key role in the transport of Aβ and the progression of AD. The decline in neuro-vascular functions leads to vessel degeneration and cerebral hypoperfusion, which ultimately affects the blood–brain barrier, and leads to an imbalance in neuron micro-environment. Dysfunction of the blood–brain barrier may lead to accumulation and deposition of Aβ in the brain. The accumulation of Aβ has been well described in transgenic mice, which over-express mutant human genes for amyloid precursor protein and presenilin-1 (APP/PS1). APP/PS1 mice gradually develop memory deficiencies that correlate with Aβs deposition [6,21,22]. Moreover, there is a strong pathological correlation between intra-cranial arterio-sclerotic vascular disease and AD. Current studies indicate that ischemia-reperfusion brain injuries can be involved in the development of AD neuro-pathology, and include the same risk factors (e.g., age, hyperlipidemia, hypertension, and diabetes), brain atrophy, neuro-inflammatory reactions, etc. [28,30,31,34].

The development of neuronal death and amyloid plaques are characteristic features of ischemic- and Alzheimer-type dementia [27]. As an effect of chronic ischemic blood–brain barrier injury, a visible connection of amyloid plaques with neuro-vasculature was observed. This neuro-pathology appears to have similar distribution and mechanisms to AD. Chronic cerebral ischemia is caused by a long-term cerebral hypoperfusion; it is a common pathological process that usually occurs in conditions, such as AD disease and vascular dementia [8]. A study of Wang *et al*. reported that chronic cerebral hypoperfusion has been associated with cognitive decline in aging and AD [41]. Current studies indicate that ischemia-reperfusion brain injury can be involved in development of AD neuro-pathology [29]. However, research on the specific clinical relationships between cerebral ischemia and Alzheimer has been rarely reported. We conducted this study to investigate the changes in neuro-vascular units after ischemia-hypoperfusion in APP/PS1 double-transgenic mice, and evaluated the role of ischemic factors in the progression of AD.

Material and methods

Animal model

This study was performed in strict compliance with local guidelines for the care and use of laboratory animals, while adhering to policies on the use of animals in neuro-scientific research released by the American Society of Neuroscience. All protocols were pre-approved by a local ethics committee. Surgery was performed under appropriate sedation, analgesia, or anesthesia, and every effort was made to minimize the distress and suffering of the animals. Group sizes were kept to the minimum number of mice that were required to obtain valid results.

APP/PS1 double-transgenic mice and C57BL mice were males, aged between 6-8 weeks, and weighing 20 ±2 g, without specific pathogens (SPF). Each group comprised 20 mice that were purchased from Beijing Huafukang Biotechnology Co., Ltd. There were five mice in each cage, and they could obtain food and water freely. They were fed adaptively for seven days with a 12-hour dark/light cycle each day. After this process, the experiment was carried out.

In the ischemic model, mice were anesthetized firstly with 4% isoflurane, maintained at 2% isoflurane through inhalation, and the skin surface was prepared by disinfection using 75% ethanol. The skin at the middle of the neck was removed and separated bluntly, the bilateral common carotid artery was exposed to about 1 cm, and the arterial blood vessel was stimulated with a temperature-controlled current of 80 mu A using an *in vivo* thrombometer (BT 87-3, Kunlun Institute of Biochemical Application Technology Development, Baotou City, China) for seven minutes to cause thrombosis. After surgery, a temperature sensor was used to measure the change in the surface temperature of the blood vessels. The temperature of distal portion of the blood vessels dropped suddenly, which indicated blood-vessel thrombosis. After surgery, 200,000 U/d of penicillin sodium was injected intramuscularly for three consecutive days to prevent infection. The mice who survived 24 hours after the establishment of the model were enrolled in the experimental study. Animal ethics requirements (ethical approval number: 2018 xlc012-2) were observed strictly during animal experiments. The animal groupings were as follows: group 1: C57BL sham

surgery group (control group), group 2: C57BL ischemic group (C57 ischemic group), group 3: APP/PS1 group (APP/PS1 group), group 4: APP/PS1 + ischemic group (APP/PS1 ischemic group).

Reagents and instruments

The following reagents and instruments were obtained and used in this study: a Morris water maze (1056001, Beijing Zhongshi Dichuang Technology Development Co., Ltd., China), a platform jumper (1049002, Beijing Zhongshi Dichuang Technology Development Co., Ltd., China), a color image processing system for image analysis of immuno-histochemical staining results (DpxView Pro, Denmark), and a transmission electron microscope (H-7500, HITACHI, Japan). Antibodies used were vascular endothelial growth factor (VEGF), angiopoietin (Ang) (Ang 1/2/3/4), basic fibroblast growth factor (bFGF), α7 sub-unit nicotinic acetylcholine receptors (α7-nAChRs), β-amyloid transporter–receptor for advanced glycation end products (RAGE), low-density lipoprotein receptor-related protein-1 (LRP-1), and amyloid β ($A\beta/A\beta_{1-42}$).

Behavioral testing

Male APP/PS1 and C57 mice were subjected to a water maze test [25] in a circular pool (60 cm in diameter and 50 cm in height). The pool was filled with water at 21-22°C to a depth of 30 cm. A hidden platform 11 cm in diameter was placed 1.5 cm under the surface of the water. The pool was divided into four quadrants, one of which contained a hidden platform. The mice were tested in the four quadrants in a fixed order. The starting location was randomized among the four quadrants, and the training was conducted once a day for five consecutive days. For the training methods, a water entry point was selected and marked from the second quadrant wall. The mice were placed into the water facing the wall. Time required for the mice to enter the water and to search for and climb the platform was recorded by an automatic video recording system (the criteria were met when the animals' limbs climbed the platform, i.e., escape latency and swimming distance). If the mice did not find the platform within three minutes, the researcher guided them to the platform for 10 seconds, and the escape latency was recorded as 180 seconds. On the afternoon of the fifth day, the platform was withdrawn, and two water entry points were selected. Then, the mice were placed into the pool facing the wall. The camera system automatically recorded the number of times the mice entered and left the original platform area within three minutes, and the swimming time and distance in the fourth quadrant of the original platform were used as indicators to evaluate the learning and memory performance of the mice.

The mice were put into the test box of platform jumper for five minutes to adapt to the environment. Then, they were placed lightly on the platform, and a copper grate was electrified. When the mice jumped off the platform and touched the copper grate, they received a shock. The normal avoidance reaction was to jump onto the platform and return to the safety zone to escape the shock. Therefore, they learned for five minutes, and the process was recorded. The number of electric shocks (the number of errors) in minutes was considered to represent successful learning. After 24 hours, the mice were placed on the jumping platform again. The latency and number of errors in five minutes (the number of times that the animals' limbs were exposed to the copper grid simultaneously) were recorded from the time the mice remained on the jumping platform to their first jump, which served as the evaluation index of memory function.

Tissue preparation

For light microscopy studies, the APP/PS1 and C57BL mice were anesthetized with 4% isoflurane and maintained at 2% isoflurane through inhalation, and were transcardially perfused with 0.1 M of phosphate-buffered saline (PBS), followed by 4% paraformaldehyde, 75 mM lysine, and 10 mM sodium metaperiodate in a 0.1-M phosphate buffer (PB). Fixed and cryo-protected brains were serially sectioned on a freezing microtome at a thickness of 40 mm in the coronal plane. For Western blot analysis and quantitative real-time polymerase chain reaction (qPCR) testing, unfixed and frozen hippocampi from the murine samples were used. For transmission electron microscopy, the sections were post-fixed in 1% osmium tetroxide in 0.1 M of PB. Then, they were block-stained with uranyl acetate, dehydrated in graded acetone, and embedded in araldite. Selected areas were cut into ultra-thin sections, and were examined under electron microscope (JEOL JEM 1400). Ink–gelatin perfusion was used to observe micro-vessels. Coronal tissue was cut into sections with a thickness of 30 µm, using

a continuous frozen section. Sections were selected from every five pieces and were collected with a patch method and natural air drying. Finally, Congo red staining was applied to observe amyloidosis of the hippocampus and cortex in three sections of the hippocampus CA-1 region at the same location.

Immuno-histochemical staining

Immuno-fluorescence analysis was performed as described by Manczak and Reddy [23]. Mouse brain tissues were fixed with a 10% formalin solution for 48-72 hours; then, they were dehydrated and embedded into paraffin, and cut into 4 µm coronary sections. Every three hippocampal slices with similar anatomical regions for each mouse were stained with each antibody. The slices were dewaxed, hydrated by gradient alcohol, repaired with a sodium citrate buffer, and blocked with normal goat serum sealing fluid. These samples were incubated with anti-$A\beta_{1-42}$ antibody and APP (anti-β amyloid 1-42 antibody [mOC64, ab201060], and anti-APP antibody [Y188, ab32136]) overnight at 4°C. HRP-labeled anti-rabbit/mouse IgG (ZSGB-BIO) was used for antigen identification, and DAB (ZSGB-BIO) staining was performed. Images of the slices were collected using Olympus cellSens (Tokyo, Japan) software and were analyzed using ImageJ (NIH) software (Media Cybernetics Inc., Rockville, MD, USA). The proportion (%) of APP-positive cells and the number of $A\beta_{1-42}$-positive cells in the CA-1 region were counted.

Overnight at 4°C, the HRP-labeled anti-rabbit/mouse IgG (ZSGB-BIO) was used to identify the antigens, and DAB (ZSGB-BIO) staining was performed. Images of the slices were collected using Olympus cellSens (Tokyo, Japan) software, and were analyzed using ImageJ (NIH) software (Media Cybernetics Inc., Rockville, MD, USA). The proportion (%) of APP-positive cells and the number of $A\beta_{1-42}$-positive cells in the CA-1 region were counted.

Enzyme-linked immunosorbent assay analysis of Aβ peptides, VEGF, angiopoietin, and FGF expression in the hippocampus and cerebrospinal fluid

Briefly, the samples were weighed and homogenized in an 8 × volume of PBS with an AEBSF protease-inhibitor cocktail set (Cat # KHB3481 and KHB3441; Invitrogen, Camarillo, CA, USA). The soluble fraction was centrifuged for 10 minutes at 4,000 × g. The pellets containing insoluble Aβ peptides were solubilized in a 5-M guanidine HCl/50 mM tris HCl solution by incubating for 3.5 hours in an orbital shaker at room temperature, to obtain an insoluble fraction. The method of collecting cerebrospinal fluid from the mice was modified, and fluid was extracted slowly (around 100-200 µl). Levels of $A\beta_{1-42}$, VEGF, Ang 1/2/3/4, and BFGF were determined by employing commercially available human enzyme-linked immunosorbent assay (ELISA) kits (Cat No.: KHB3481 and KHB3441, Invitrogen, Camarillo, CA, USA) [26]. Data obtained from the tissue homogenates were expressed as picograms of Aβ, VEGF, Ang, and BFGF content per mg of total protein (pg/mg).

Transmission electron microscopy

Brief trans-cardiac perfusion with 0.9% saline was performed to remove the circulating blood followed by perfusion with a fixative containing 2% paraformaldehyde and 2.5% glutaraldehyde in a 0.1-M phosphate buffer (pH = 7.4). Then, the brains were dissected and post-fixed in a fresh fixative for 24 hours at 4°C. Coronal sections (100 µm thick) were cut using a Leica VT1000 vibrating-blade vibratome, and in coronal section of interest, the subiculum of hippocampal formation (termed the hippocampus) was micro-dissected. The samples were washed in a cacodylate buffer containing 2 mM of calcium chloride and were post-fixed for one hour with reduced osmium (OsO_4 1% and $K_4Fe(CN)_6$ 1.5%). Then, they were incubated in 1% tannic acid in a 0.1-M cacodylate buffer for one hour and overnight in 1% uranyl acetate in water. The samples were dehydrated at room temperature with different grades of ethanol (from 20% to 100% for five minutes each), infiltrated with TAAB low-viscosity resin (TAAB Laboratories Equipment, UK), and polymerized for 24 hours at 60°C. Then, ultrathin sections (70 nm) were cut using a Reichert-Jung ultracut E ultramicrotome (Reichert Technologies Life Sciences, USA); they were mounted on Athene 200-mesh thin-bar copper grids (Agar Scientific, UK) and were visualized by FEI Tecnai 12 BioTwin transmission electron microscope (FEI, USA) using a Gatan Orius SC1000 camera (Gatan, USA).

Western blot analysis

Aliquots of hippocampus homogenate containing 15 mg of protein per sample were analyzed using

the Western blot method [24]. In brief, samples were placed in a sample buffer (0.5 m Tris–HCl; pH = 6.8; 10% glycerol, 2% (w/v) SDS, 5% (v/v) 2-mercaptoethanol, and 0.05% bromophenol blue) and were denatured by boiling at 95-100°C for five minutes. Then, the samples were separated by electrophoresis on 10-15% acrylamide gels, and proteins were transferred to PVDF membranes, using a trans-blot apparatus. Membranes were blocked overnight with 5% non-fat milk dissolved in TBS-T buffer (50 mM tris; 1.5% NaCl, 0.05% tween 20; pH = 7.5). Then, they were incubated with primary antibodies. After overnight incubation, the blots were washed thoroughly in a TBS-T buffer, and were incubated for one hour with a peroxidase-conjugated IgG secondary antibody (1 : 2,000). Immunoreactive protein was detected using a chemiluminescence-based detection kit. Protein levels were determined by densitometry using a ChemiDoc XRS+ molecular imaging detection system (Bio-Rad), with ImageLab image analysis software. Measurements were expressed as arbitrary units, and all results were normalized to GAPDH, unless otherwise stated.

Reverse-transcription polymerase chain reaction analysis

After tissue processing, a MiniBEST Universal RNA extraction kit (TaKaRa, Dalian, China) was used to extract the total RNA according to the manufacturer's instructions. RNA concentration was determined according to 260/280 nm absorbance using a NanoDrop spectrophotometer (ND-1000, Thermo Fisher Scientific, Waltham, MA, USA). RNA was reverse-transcribed into cDNA using a PrimeScript™ RT reagent kit (036A) (TaKaRa, RR047B), and cDNA was quantified using an SYBR® Premix Ex Taq™ II (TaKaRa, RR82LR) reagent [23]. Synthesis of the target gene primers for RT2-PCR is shown in Table I. Data were normalized to GAPDH level.

Statistical analysis

We used SPSS v.22.0 (IBM, Chicago, USA) software to conduct a statistical analysis. Continuous variables of normal distribution were expressed as mean ± standard deviation, continuous variables of non-normal distribution were expressed as median (interquartile range [IQR]), and categorical variables were expressed as frequency (percentage [%]). For multiple comparisons, when each datum conformed to a normal distribution, each value was compared using one-way analysis of variance test following Dunnett test, while non-normally distributed continuous data were compared using non-parametric tests. Counting data were analyzed using χ^2 test. A value of $p < 0.05$ was considered statistically significant.

Results

Influence of ischemia on spatial learning and memory ability of mice

To examine learning and memory function, a Morris water maze was used in all four groups. Table II shows that the number of crossings, the swimming time, and the swimming distance of the mice in the APP/PS1 group ($p < 0.05$), the APP/PS1 ischemic group ($p < 0.01$), and the C57 ischemic group ($p < 0.05$) were significantly less than those in the control group, which

Table I. Primer sequence of each gene

Primer name	Primer sequence (5' to 3')	Product size (bp)
VEGF upstream primer	ATCATGCGGATCAAACCTCACC	101
VEGF downstream primers	GGCTTTGTTCTGTCTTTCTTTGGTC	
RAGE upstream primer	GACGGGACTCTTTACACTGCG	191
RAGE downstream primers	CACCTTCAGGCTCAACCAACA	
α7-nAChRs upstream primer	CTGGCTTTGCTGGTATTCTTG	204
α7-nAChRs downstream primers	CACAATCACTGTCACGACCACT	
LRP1 upstream primer	TTCTGGTATAAGCGGCGAGTC	167
LRP1 downstream primers	TCAGGGTCAAGGGCAAAATC	
Aβ1-42 upstream primer	TGGTGGACCCCAAGAAAGC	184
Aβ1-42 downstream primers	GCCAAGACATCGTCGGAGTAG	
ACTIN upstream primer	CGTTGACATCCGTAAAGACCTC	159
ACTIN downstream primers	ACAGAGTACTTGCGCTCAGGAG	

Table II. Effect of the method of benefiting qi and activating blood circulation on the spatial learning and memory ability of APP/PS1 dual-transgenic ischemic mice ($\bar{x} \pm s$)

Group	Dose (g/kg·d)	*n*	Number of crossings (times)	Swimming time (*s*)	Swimming distance (cm)
C57 sham-operated group (control group)	–	16	7.12 ±1.27	46.89 ±12.23	318.34 ±89.23
C57 ischemic group	–	16	5.18 ±1.32**	39.12 ±10.35**	252.10 ±101.43**
APP/PS1 group	–	16	4.17 ±2.12**	37.23 ±9.89**	275.17 ±97.34**
APP/PS1 ischemic group	–	16	3.37 ±1.72▲	33.02 ±11.23▲▲	237.23 ±98.32▲

*Compared with control group: * $p < 0.05$, ** $p < 0.01$; Compared with APP/PS1 group: ▲ $p < 0.05$, ▲▲ $p < 0.01$*

Table III. Effect of the method of benefiting qi and activating blood circulation on the platform test of APP/PS1 dual-transgenic ischemic mice ($\bar{x} \pm s$)

Group	Dose (g/kg·d)	*n*	Number of electric shocks (times)	Latency (s)
C57 sham-operated group (control)	–	15	1.27 ±1.16	226.45 ±53.12
C57 ischemic group	–	15	2.20 ±1.37*	179.23 ±55.29*
APP/PS1 model group	–	14	2.59 ±1.27*	167.65 ±61.20**
APP/PS1 ischemic group	–	15	3.13 ±1.70**	156.78 ±54.87**

*Compared with C57 sham-operated group (control): * $p < 0.05$, ** $p < 0.01$*

indicates that the mouse models were successful. The number of crossings, swimming time, and swimming distance in the APP/PS1 ischemic group were lower than those in the APP/PS1 group ($p < 0.05$).

Comparing the number of platform jumping errors, there was no significant difference in the number of errors between the groups of mice ($p > 0.05$), but the trend of the model group showed an increasing number of errors. Compared with the C57 sham operation group, the incubation periods of the APP/PS1 model group and the APP/PS1 ischemic group were significantly shorter ($p < 0.01$). The results are shown in Table III. The number and latency of step-down in the APP/PS1 group ($p < 0.01$) and C57 ischemic group ($p < 0.05$) were significantly longer than those of the control group, which indicates that the models in the different groups were successful. Compared with the control group, the number of errors and the latency in the APP/PS1 group and the APP/PS1 ischemic group increased significantly ($p < 0.01$), although memory function was worse.

HE staining observes pathological form of ischemic mouse brain tissue

Hematoxylin-eosin (HE) staining can show general morphological and structural characteristics of various tissues or cells. Neurons in the CA-1 region of the hippocampus of the C57 sham-operated mice were uniformly stained, large in number, neatly and densely arranged, and vacuolar degeneration and necrosis were uncommon; the CA-1 region of the hippocampus of the mice in the C57 ischemic group did not change much. The number of neurons in the CA-1 region of the hippocampus of the mice in the APP/PS1 double-transgenic model group was significantly reduced; some cell bodies were shrunk, the arrangement was disordered, extra-cellular spaces were enlarged, and nuclear membrane was unclear. The APP/PS1 double-transgenic model in the ischemic group had fewer neurons in the hippocampus CA-1 region, it exhibited partial atrophy, part of the cell body was shrunk, extra-cellular spaces were enlarged, cell structures were fuzzy, and there was more severe damage than in the APP/PS1 model group. The results are shown in Figure 1.

Observation of mouse brain tissue amyloids using Congo red staining

The brain tissues of the mice in the control group and the C57 ischemic group were relatively clear, and no positive staining was observed. In the APP/PS1 group, there were scattered orange-red sediments on the upper edge of the cortex and hippocampus, which were mostly irregular in shape, with different sizes and uneven staining. Among them, the hippocampus was densely distributed. The red deposits in the cerebral cortex of the APP/PS1 ischemic group exhibited a certain increase, and scattered red sediments appeared in the upper margin and the hippocampus (Fig. 2).

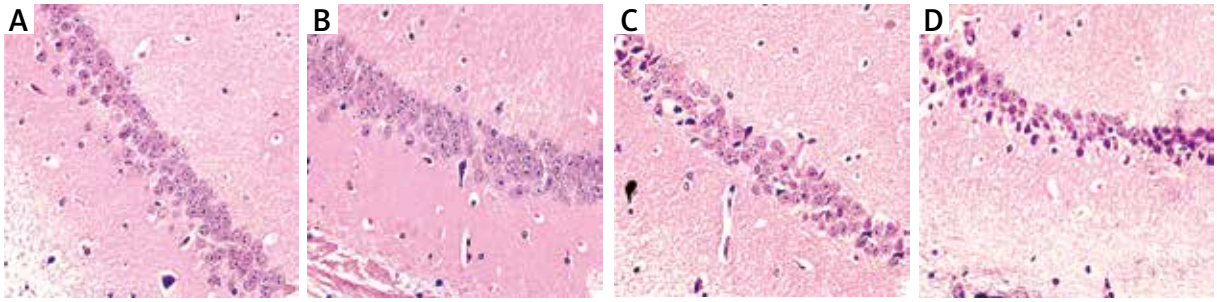

Fig. 1. Observation of pathological morphology in mouse brain tissue (HE 400×). **A**) C57 sham surgery group (control group); **B**) C57 ischemic group; **C**) APP/PS1 group; **D**) APP/PS1 ischemic group.

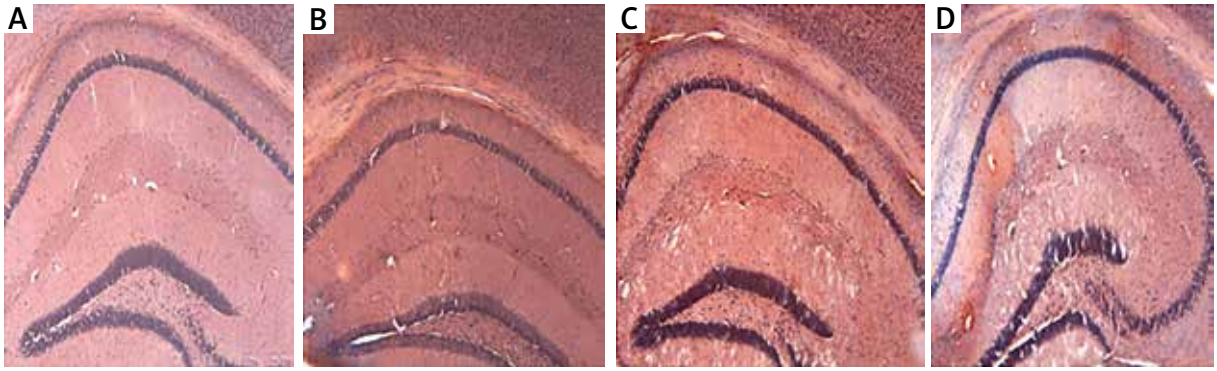

Fig. 2. Observation of amyloid stylus in mouse brain tissue (Congo red stain 40×). **A**) C57 sham surgery group (control group); **B**) C57 ischemic group; **C**) APP/PS1 group; **D**) APP/PS1 ischemic group.

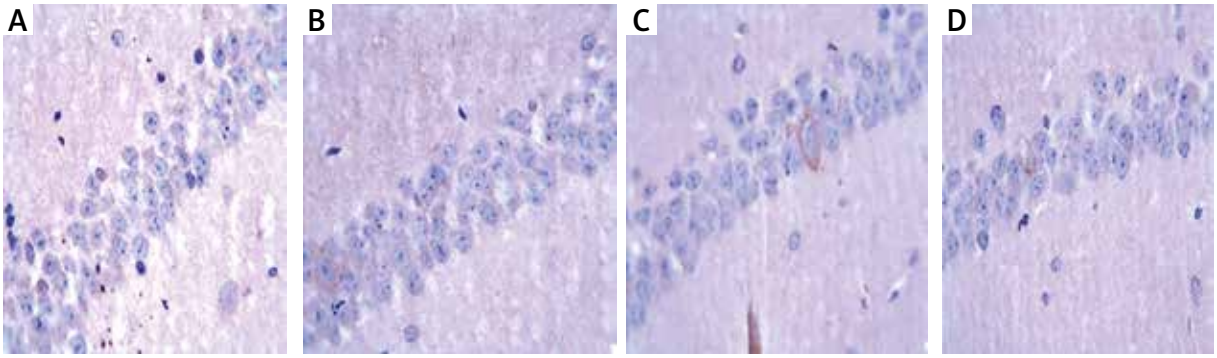

Fig. 3. Immuno-histochemistry of APP in hippocampus of mice (APP 400×). **A**) C57 sham surgery group (control group); **B**) C57 ischemic group; **C**) APP/PS1 group; **D**) APP/PS1 ischemic group.

Immuno-histochemical detection of the hippocampus in each group

The immuno-histochemical detection of the hippocampus showed that the APP/PS1 group and APP/PS1 ischemic group presented an increase in the APP positive expression area compared with the APP/PS1 group (Fig. 3). Additionally, the APP/PS1 group and APP/PS1 ischemic group had an increased Aβ-positive expression area compared with the APP/PS1 model group (Fig. 4).

Enzyme-linked immunosorbent assay to detect Aβ content in the hippocampus and the cerebrospinal fluid of each group

The ELISA results showed that compared with the control group, the C57 ischemic group had a slight increase in cerebrospinal fluid Aβ content, but there was no statistically significant difference ($p > 0.05$). Compared with the C57 ischemic group,

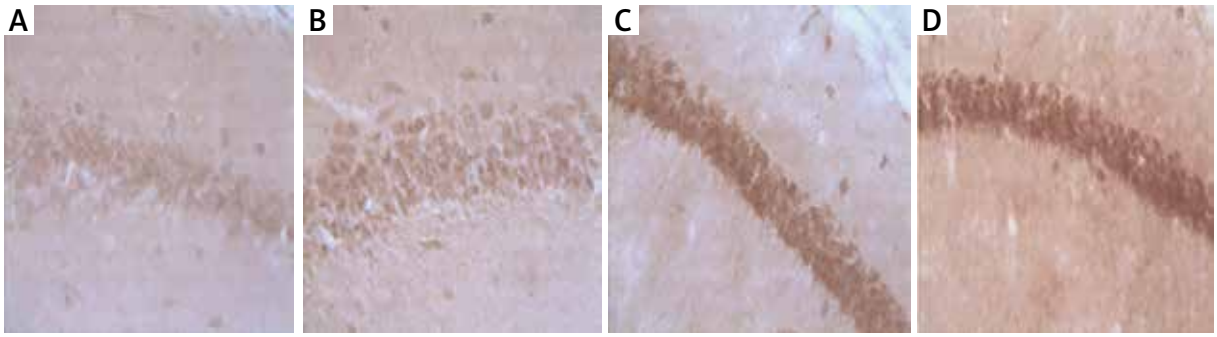

Fig. 4. Immuno-histochemistry of $A\beta_{1-42}$ in hippocampus of mice ($A\beta_{1-42}$ 400×). **A**) C57 sham surgery group (control group); **B**) C57 ischemic group; **C**) APP/PS1 group; **D**) APP/PS1 ischemic group.

Table IV. Enzyme-linked immunosorbent assay to detect the Aβ content in the hippocampus and cerebrospinal fluid of each group of mice ($\bar{x} \pm s$)

	Hippocampus	Cerebrospinal fluid
C57 sham-operated (control) group	0.085 ±0.019	0.795 ±0.249
C57 ischemic group	0.136 ±0.026	1.022 ±0.170
APP/PS1 model group	0.157 ±0.013**	1.225 ±0.273
APP/PS1 ischemic group	0.185 ±0.021**	1.521 ±0.135

*Compared with C57 ischemic group: ** $p < 0.01$*

the Aβ content of the mice in the APP/PS1 group and the APP/PS1 ischemic group increased significantly ($p < 0.01$). The results are shown in Table IV.

Ultrastructure observations of the neuro-vascular units in each group

In the control group, the nuclear membrane was intact, chromatin structure and quantity were normal, the morphology and distribution of the mitochondria, endoplasmic reticulum, Golgi apparatus, and nuclei were basically normal, and autophagosomes were rare around nuclei. There were more mitochondrial vacuoles in the hippocampal neurons in the APP/PS1 group of mice, and the structure was relatively intact. Mitochondrial vacuoles in the hippocampal neurons of the APP/PS1 ischemic group increased significantly, and the vascular wall proliferated. The APP/PS1 ischemic group had significantly more empty mitochondria in the hippocampal nerve cells, and the blood-vessel wall proliferated (as shown in Fig. 5).

Enzyme-linked immunosorbent assay to detect the contents of VAGF, angiogenin, and FGF in each group

The results showed that compared with the control group, the VEGF content of the C57 ischemic group significantly increased ($p > 0.01$). Compared with the APP/PS1 group, the VEGF content of the mice in the APP/PS1 ischemic group increased significantly ($p < 0.05$). However, Ang and BFGF had no significant difference in the content of each group ($p > 0.05$). The results are presented in Table V.

Western blot for detecting the expression of VEGF, RAGE, LRP-1, α7-nAChRs, and $A\beta_{1-42}$ proteins in the brain tissue of each group

The results showed that compared with the C57 sham operation group, the expression of VEGF in the brain tissue of the C57 ischemic group increased to a certain extent ($p < 0.05$). In the expression of RAGE, LRP-1, α7-nAChRs, and $A\beta_{1-42}$ in the C57 ischemic group, RAGE and LRP-1 were relatively low without any significant difference. Compared with the C57 sham surgery group, the expression of $A\beta_{1-42}$, RAGE, and α7-nAChRs proteins in the APP/PS1 group and the APP/PS1 ischemic group significantly increased to varying degrees ($p < 0.05$). Compared with the C57 ischemic group, the expression of $A\beta_{1-42}$, RAGE, and α7-nAChRs proteins in the APP/PS1 ischemic group increased ($p < 0.05$). The results are given in Figure 6.

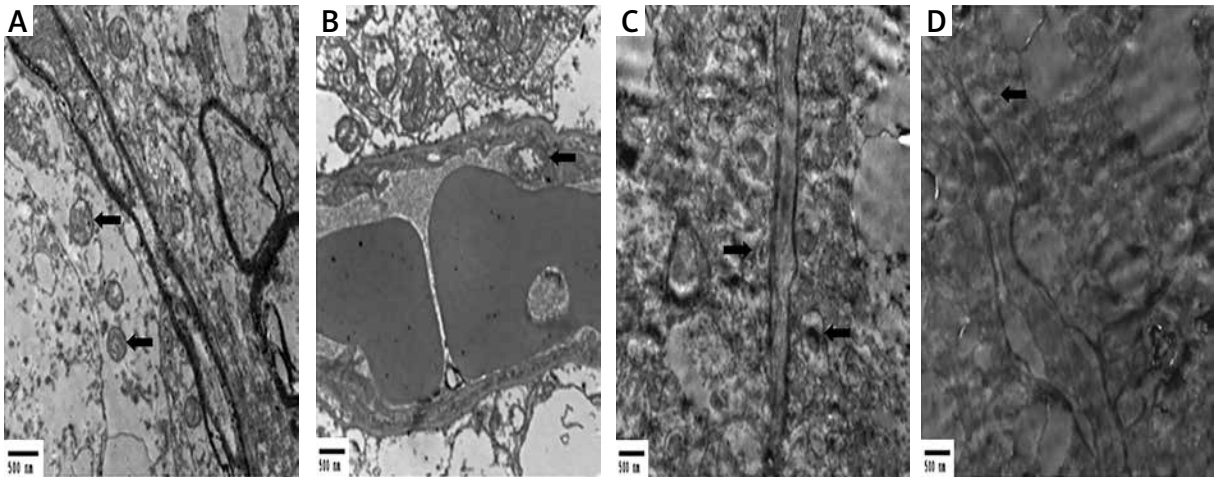

Fig. 5. Electron microscopic observation of neuro-vascular units in hippocampus of mice. **A**) C57 sham surgery group (control group); **B**) C57 ischemic group; **C**) APP/PS1 group; **D**) APP/PS1 ischemic group. Scale bars = 500 nm.

Table V. Effect of the method of benefiting qi and activating blood circulation on the content of VEGF, Ang, and BFGF in APP/PS1 dual-transgenic ischemic mice (n = 5;)

Group	Dose (g/kg·d)	VEGF (ng/mg)	Ang (ng/mg)	BFGF (ng/mg)
C57 sham-operated group (control)	–	9.59 ±1.23	1.58 ±0.49	6.35 ±2.06
C57 ischemic group	–	12.36 ±2.42*	1.49 ±0.16	6.56 ±0.54
APP/PS1 model group	–	6.80 ±1.69*	1.22 ±0.83	5.81 ±2.39
APP/PS1 ischemic group	–	10.53 ±2.96	1.42 ±0.54	5.57 ±1.57

*Compared with C57 ischemic group: * $p < 0.05$*

Reverse-transcription polymerase chain reaction for detecting the expression of VEGF, RAGE, LRP-1, α7-nAChRs, and $A\beta_{1\text{-}42}$ in the brain tissue of each group

The results of reverse-transcription polymerase chain reactions showed that compared with the control group, the expression of the VEGF gene in the brain tissue of the C57 ischemic group increased to a certain extent ($p < 0.05$), and the C57 ischemic group had relatively lower gene expression levels of RAGE, LRP-1, α7-nAChRs, and $A\beta_{1\text{-}42}$ ($p > 0.05$). Compared with the control group, the expression of $A\beta_{1\text{-}42}$, RAGE, and α7-nAChRs genes in the APP/PS1 group and the APP/PS1 ischemic group increased to varying degrees ($p < 0.05$). In comparison with the C57 ischemic group, the expression of $A\beta_{1\text{-}42}$, RAGE, and α7-nAChRs genes in the APP/PS1 ischemic group also increased ($p < 0.05$).

Discussion

In the present study, we investigated the effects of ischemia on the neuro-vascular units of transgenic mice, and the role of ischemia-hypoperfusion in a dual-transgenic dementia mouse model. The theory of Aβ is one of the key mechanisms in AD research. The misfolding and progressive accumulation of amyloid peptides (A) in soluble assemblies and amyloid plaques may represent critical pathogenic factors in AD [2,7,18]. Our data showed that the positive expression area of APP and Aβ in the APP/PS1 group was significantly higher than that in the C57 ischemic group. Precipitated Aβ is neuro-toxic, and causes synaptic changes, Tau protein phosphorylation, loss of transmitters, glial hyperplasia, cerebral micro-angiopathy, inflammatory reactions, etc. These reactions can lead to successive pathological damage, such as plaque formation, neuro-fibrillary tangles, and eventually, AD [5,17,37,38]. Behavior of different mouse groups was tested using Morris water maze. The results showed that the number of crossings, swimming time, and swimming distance of the APP/PS1 mouse group were worse than those of the ischemic group. The result of step-down test showed that the number of step-ups and latency of the APP/PS1 mice were higher than those of the

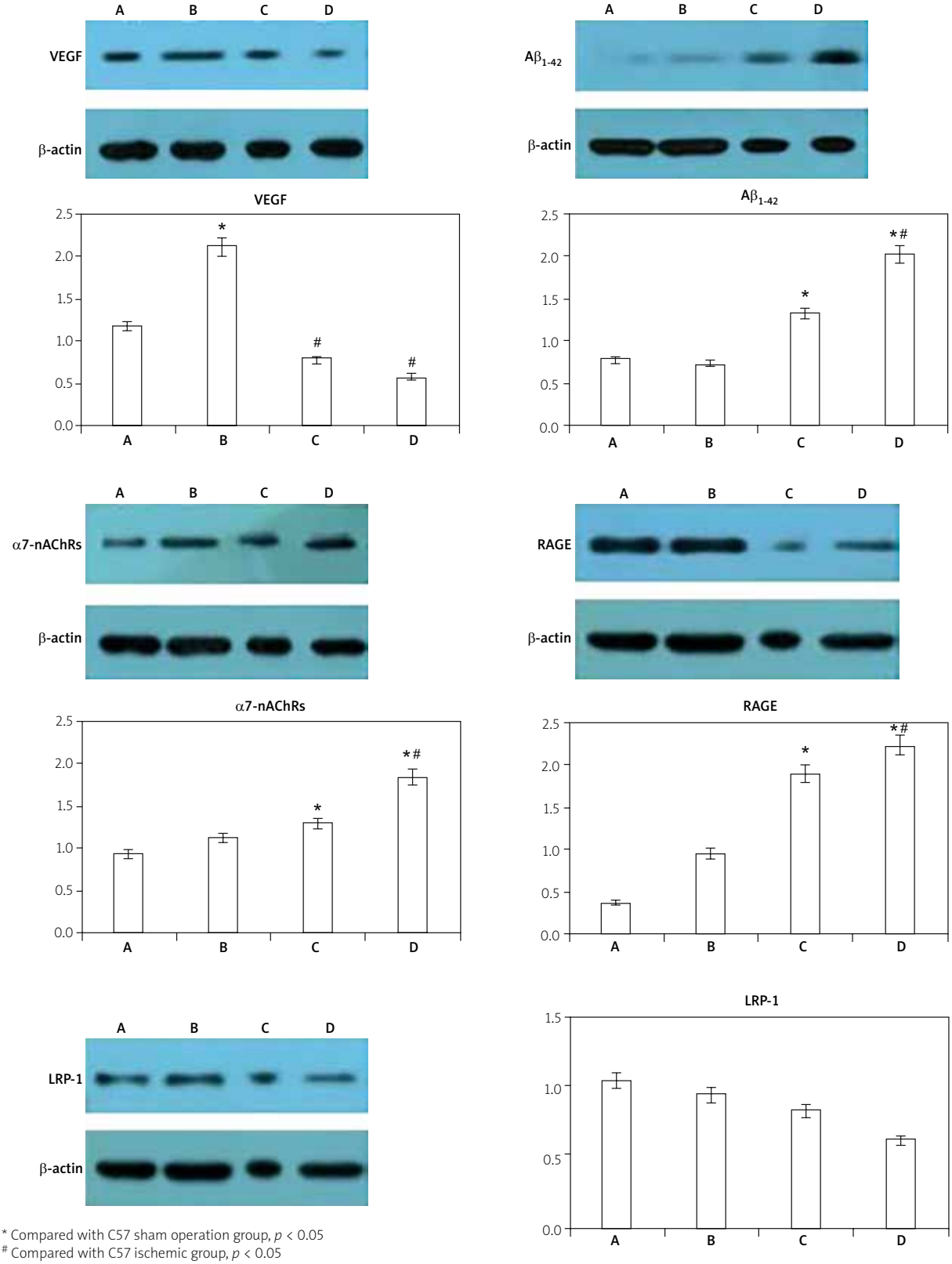

* Compared with C57 sham operation group, $p < 0.05$
\# Compared with C57 ischemic group, $p < 0.05$

Fig. 6. Detection of protein expression in mice. A – C57 sham surgery group (control group); B – C57 ischemic group; C – APP/PS1 group; D – APP/PS1 ischemic group.

ischemic mice. The accumulation of Aβ resulted in a decrease in the learning and memory function in the mice with AD.

The deposition of Aβ also led to cholinergic nerve damage, which affected the synthesis, release, transport, and metabolism of choline [32,33,36]. Nicotinic acetylcholine receptors (nAChRs) are widely distributed throughout the central nervous system, being expressed in neurons and non-neuronal cells, where they participate in a variety of physiological responses, such as memory, learning, locomotion, attention, etc. Alpha 7 neuronal nicotinic acetylcholine receptors (nAChRs) are involved in essential physiological functions, and play a role in various disorders, such as AD. A Western blot analysis showed that the expression of α7-nAChRs protein in the APP/PS1 ischemic group was slightly higher than in the C57 ischemic group. Interestingly, the effect was observed in the presence of structurally unrelated inhibitor of the muscarinic receptor, pirenzepine [9], demonstrating that the inhibition of muscarinic activity is the primary cause for upregulation of Aβ transport, which reduces pathological phenotypes in AD mouse models.

A neuro-vascular unit is a functional unit composed of neurons, glial cells, and endothelial cells. The aggregation of Aβ leads to a decline in neuro-vascular function, a further decomposition in neuro-vascular coupling, vascular degeneration, cerebral hypoperfusion, etc., which ultimately affects the function of blood-brain barrier and leads to an imbalance in neuronal micro-environment. The dysfunction of blood-brain barrier leads to accumulation and deposition of Aβ in the brain. During the test, HE staining showed that the number of neurons in the hippocampal CA-1 region of the APP/PS1 mice was significantly diminished, some of the cell bodies were reduced, the boundary of nuclear membrane was unclear, and the extra-cellular space was enlarged and disordered. The worst result was in the number of neurons, cell bodies, extra-cellular spaces, and cell structures in the hippocampal CA-1 region of the APP/PS1 ischemic group. Compared with the APP/PS1 mouse group, ischemia aggravated cell damage. Congo red staining showed that orange-red sediments were scattered in the upper cortex and the hippocampus of the APP/PS1 mice, and indicated mostly irregular, differently sized, and uneven staining. The hippocampus was particularly densely distributed. Red deposits in the cortex of the APP/PS1 ischemic mouse group increased, and both the upper margin and hippocampus appeared [19,40]. There were more mitochondrial vacuoles in the hippocampal neurons of the APP/PS1 mice, although the structure was relatively intact. The data also showed that the mitochondrial vacuoles in the hippocampal neurons of the APP/PS1 ischemic group increased significantly, and the vascular wall proliferated.

The translocation of Aβ across the blood-brain barrier was accomplished mainly by the receptor of advanced glycation end products (RAGE) and low-density lipoprotein receptor-related protein-1 (LRP-1) RAGE/LRP-1 system. Compared with the C57 ischemic mouse group, Western blot detection showed that the expression of RAGE protein increased, while the expression of LRP-1 decreased significantly in the APP/PS1 ischemic group of mice. The reverse-transcription polymerase chain reaction showed that in the APP/PS1 ischemic group, RAGE increased and LRP-1 decreased. The receptor of advanced glycation end products mediates the transport of Aβ into the brain, while LRP-1 mediates the transport of Aβ out of the brain. In patients with AD, the expression of RAGE on the blood-brain barrier is up-regulated. The combination of RAGE and Aβ on the membrane of the brain's micro-vascular endothelial cells can promote the accumulation of Aβ in the brain after crossing the blood-brain barrier. Moreover, as a receptor of Aβ, RAGE mediates both neurological impairment and vascular dysfunction [16,20]. Additionally, the results revealed that the expression of LRP-1 in the micro-vascular endothelial brain cells of mice with AD was negatively correlated with the number of Aβ-positive vessels.

Vascular endothelial growth factor VEGF promotes vascular endothelial cell proliferation and neo-vascularization, and is essential to the clearance of Aβ. In the body studies, VEGF has a protective effect on choline energy neurons, inducing blood vessels, and reduces $A\beta_{1-42}$ deposition, improve cognitive function in transgenic mice. Ang is a glycoprotein that belongs to a specific angiogenesis. The role of FGF in blood vessels is mainly promoted by vascular endothelial cell proliferation, migration, and lumen formation. According to ELISA, the concentration of VEGF in the cerebrospinal fluid of the APP/PS1 group was lower than that of the C57 ischemic group, while the concentration of VEGF in the APP/PS1 ischemic group was slightly higher

than in the APP/PS1 group. Moreover, Ang and BFGF had no significant difference in the content of each group. The results showed that the concentration of VEGF in the APP/PS1 ischemic group had a strong correlation with ischemia. A Western blot analysis further showed that ischemia was an effective stimulating factor for VEGF. It is speculated that under the condition of low perfusion, the continuous deposition of VEGF in amyloid plaques may lead to a decrease in the utilization of VEGF, thus promoting neuro-degenerative diseases and vascular dysfunction in progressive AD.

In conclusion, this study further confirmed that there may be a co-promoting mechanism in the pathological mechanism of AD and vascular dementia. Ischemia deteriorates the learning and memory functions of transgenic mice, aggravates the damage of neuro-vascular units, and a further deterioration in neuro-vascular units. At the same time, ischemia is an effective stimulating factor for the release of VEGF.

Ethical statement

This study was conducted in accordance with the Declaration of Helsinki, and was approved by ethics committee of our hospital.

Funding

The study received a funding from the National Natural Science Foundation of China (No. 81503450).

Availability of data and materials

The datasets used and analyzed during the current study are available from the corresponding author on reasonable request.

Disclosure

The authors conflict of interest.

References

1. Cacabelos R, Torresllas C. Epigenetic drug discovery for Alzheimer's disease. Expert Opin Drug Discov 2018; 9: 1059-1086.
2. Cappai R, Barnham KJ. Delineating the mechanism of Alzheimer's disease Aβ peptide neurotoxicity. Neurochem Res 2008; 33: 526-532.
3. Chen YG. Research progress in the pathogenesis of Alzheimer's disease. Chin Med J (Engl) 2018; 131: 1618-1624.
4. Cummings J, Ritter A, Zhong K. Clinical trials for disease-modifying therapies in Alzheimer's disease: a primer, lessons learned, and a blueprint for the future. J Alzheimers Dis 2018; 64: S3-S22.
5. Das BC, Dasgupta S, Ray SK. Potential therapeutic roles of retinoids for prevention of neuroinflammation and neurodegeneration in Alzheimer's disease. Neural Regen Res 2019; 14: 1880-1892.
6. Dickey CA, Gordon MN, Mason JE, Wilson NJ, Diamond DM, Guzowski JF, Morgan D. Amyloid suppresses induction of genes critical for memory consolidation in APP + PS1 transgenic mice. J Neurochem 2004; 88: 434-442.
7. Evin G, Weidemann A. Biogenesis and metabolism of Alzheimer's disease Aβ amyloid peptides. Peptides 2002; 23: 1285-1297.
8. Gao M, Li L, Peng Z, Yu G. Neuroprotective effect of Curcumin involved in increasing the protein levels of UCP2 and inhibiting oxidative stress induced by chronic cerebral ischemia in vitro. Mol Neurodegener 2012; 7: S26-S26.
9. Gao ZG, Toti KS, Campbell R, Suresh RR, Yang HJ, Jacobson KA. Allosteric antagonism of the A(2A) adenosine receptor by a series of bitopic ligands. Cells 2020; 9: 1200.
10. Kandimalla R, Manczak M, Fry D, Suneetha Y, Sesaki H, Reddy PH. Reduced dynamin-related protein 1 protects against phosphorylated Tau-induced mitochondrial dysfunction and synaptic damage in Alzheimer's disease. Hum Mol Genet 2016; 25: 4881-4897.
11. Kandimalla R, Manczak M, Yin X, Wang R, Reddy PH. Hippocampal phosphorylated tau induced cognitive decline, dendritic spine loss and mitochondrial abnormalities in a mouse model of Alzheimer's disease. Hum Mol Genet 2018; 27: 30-40.
12. Kandimalla R, Reddy PH. Therapeutics of neurotransmitters in Alzheimer's disease. J Alzheimers Dis 2017; 57: 1049-1069.
13. Kandimalla R, Thirumala V, Reddy PH. Is Alzheimer's disease a type 3 diabetes? A critical appraisal. Biochim Biophys Acta Mol Basis Dis 2017; 1863: 1078-1089.
14. Kandimalla RJ, Anand R, Veeramanikandan R, Wani WY, Prabhakar S, Grover VK, Bharadwaj N, Jain K, Gill KD. CSF ubiquitin as a specific biomarker in Alzheimer's disease. Curr Alzheimer Res 2014; 11: 340-348.
15. Kandimalla RJ, Prabhakar S, Wani WY, Kaushal A, Gupta N, Sharma DR, Grover VK, Bhardwaj N, Jain K, Gill KD. CSF p-Tau levels in the prediction of Alzheimer's disease. Biol Open 2013; 2: 1119-1124.
16. Kim DE, Priefer R. Therapeutic potential of direct clearance of the amyloid-β in Alzheimer's disease. Brain Sci 2020; 10: 93.
17. Kim MS, Kim Y, Choi H, Kim W, Park S, Lee D, Kim DK, Kim HJ, Choi H, Hyun DW, Lee JY, Choi LY, Lee DS, Bae JW, Mook-Jung I. Transfer of a healthy microbiota reduces amyloid and tau pathology in an Alzheimer's disease animal model. Gut 2020; 69: 283-294.
18. Kuperstein I, Broersen K, Benilova I, Rozenski J, Jonckheere W, Debulpaep M, Vandersteen A, Segers-Nolten I, Van Der Werf K, Subramaniam V, Braeken D, Callewaert G, Bartic C, D'Hooge R, Martins IC, Rousseau F, Schymkowitz J, De Strooper B. Neurotoxicity of Alzheimer's disease Aβ peptides is induced by small changes in the Aβ42 to Aβ40 ratio. EMBO J 2014; 29: 3408-3420.
19. Lubitz I, Ricny J, Atrakchi-Baranes D, Shemesh C, Kravitz E, Liraz-Zaltsman S, Maksin-Matveev A, Cooper I, Leibowitz A, Uribarri J, Schmeidler J, Cai WJ, Kristofikova Z, Ripova D, LeRoith D, Schnaider-Beeri M. High dietary advanced glycation end products are associated with poorer spatial learning and accelerated

Aβ deposition in an Alzheimer mouse model. Aging Cell 2016; 15: 309-316.
20. Lue LF, Walker DG, Brachova L, Beach TG, Rogers J, Schmidt AM, Stern DM, Yan SD. Involvement of microglial receptor for advanced glycation endproducts (RAGE) in Alzheimer's disease: identification of a cellular activation mechanism. Exp Neurol 2001; 171: 29-45.
21. Manczak M, Kandimalla R, Fry D, Sesaki H, Reddy PH. Protective effects of reduced dynamin-related protein 1 against amyloid beta-induced mitochondrial dysfunction and synaptic damage in Alzheimer's disease. Hum Mol Genet 2016; 25: 5148-5166.
22. Manczak M, Kandimalla R, Yin X, Reddy PH. Hippocampal mutant APP and amyloid beta-induced cognitive decline, dendritic spine loss, defective autophagy, mitophagy and mitochondrial abnormalities in a mouse model of Alzheimer's disease. Hum Mol Genet 2018; 27: 1332-1342.
23. Manczak M, Reddy PH. Mitochondrial division inhibitor 1 protects against mutant huntingtin-induced abnormal mitochondrial dynamics and neuronal damage in Huntington's disease. Hum Mol Genet 2015; 24: 7308-7325.
24. Mockett BG, Guévremont D, Elder MK, Parfitt KD, Peppercorn K, Morrissey J, Singh A, Hintz TJ, Kochen L, Dieck ST, Schuman E, Tate WP, Williams JM, Abraham WC. Glutamate receptor trafficking and protein synthesis mediate the facilitation of LTP by secreted amyloid precursor protein-alpha. J Neurosci 2019; 39: 3188-3203.
25. Morris R. Developments of a water-maze procedure for studying spatial learning in the rat. J Neurosci Methods 1984; 11: 47-60.
26. Peng Y, Sun J, Hon S, Nylander AN, Xia W, Feng Y, Wang X, Iemere CA. L-3-n-butylphthalide improves cognitive impairment and reduces amyloid-beta in a transgenic model of Alzheimer's disease. J Neurosci 2010; 30: 8180-8189.
27. Pluta R, Amek MU. Brain ischemia and ischemic blood-brain barrier as etiological factors in sporadic Alzheimer's disease. Neuropsychiatr Dis Treat 2008; 4: 855-864.
28. Pluta R, Ułamek M, Jabłoński M. Alzheimer's mechanisms in ischemic brain degeneration. Anat Rec 2009; 292: 1863-1881.
29. Pluta R, Ułamek-Kozioł M, Januszewski S, Czuczwar SJ. Participation of amyloid and tau protein in neuronal death and neurodegeneration after brain ischemia. Int J Mol Sci 2020; 21: 4599.
30. Pluta R. Brain ischemia: Alzheimer's disease mechanisms. Nova Science Publishers, New York, NY, USA 2019; 311.
31. Radenovic L, Nenadic M, Ułamek-Kozioł M, Januszewski S, Czuczwar SJ, Andjus PR, Pluta R. Heterogeneity in brain distribution of activated microglia and astrocytes in a rat ischemic model of Alzheimer's disease after 2 years of survival. Aging (Albany NY) 2020; 12: 12251-12267.
32. Roher AE, Weiss N, Kokjohn TA, Kuo YM, Kalback W, Anthony J, Watson D, Luehrs DC, Sue L, Walker D, Emmerling M, Goux W, Beach T. Increased A beta peptides and reduced cholesterol and myelin proteins characterize white matter degeneration in Alzheimer's disease. Biochemistry 2002; 41: 11080-11090.
33. Sakai K, Boche D, Carare R, Johnston D, Holmes C, Love S, Nicoll JAR. Aβ immunotherapy for Alzheimer's disease: effects on apoE and cerebral vasculopathy. Acta Neuropathol 2014; 128: 777-789.
34. Salminen A, Kauppinen A, Kaarniranta K. Hypoxia/ischemia activate processing of amyloid precursor protein: Impact of vascular dysfunction in the pathogenesis of Alzheimer's disease. J Neurochem 2017; 140: 536-549.
35. Schelke MW, Attia P, Palenchar DJ, Kaplan B, Mureb M, Ganzer CA, Scheyer O, Rahman A, Kachko R, Krikorian R, Mosconi L, Isaacson RS. Mechanisms of risk reduction in the clinical practice of Alzheimer's disease prevention. Front Aging Neurosci 2018; 10: 96.
36. Sun SW, Nishioka C, Labib W, Liang HF. Axonal terminals exposed to amyloid-β may not lead to pre-synaptic axonal damage. J Alzheimers Dis 2015; 45: 1139-1148.
37. Theofilas P, Ehrenberg AJ, Nguy A, Thackrey JM, Dunlop S, Mejia MB, Alho AT, Paraizo Leite RE, Rodriguez RD, Suemoto CK, Nascimento CF, Chin M, Medina-Cleghorn D, Cuervo AM, Arkin M, Seeley WW, Miller BL, Nitrini R, Pasqualucci CA, Filho WJ, Rueb U, Neuhaus J, Heinsen H, Grinberg LT. Probing the correlation of neuronal loss, neurofibrillary tangles, and cell death markers across the Alzheimer's disease Braak stages: a quantitative study in humans. Neurobiol Aging 2018; 61: 1-12.
38. Uddin MS, Mamun AA, Labu ZK, Hidalgo-Lanussa O, Barreto GE, Ashraf GM. Autophagic dysfunction in Alzheimer's disease: cellular and molecular mechanistic approaches to halt Alzheimer's pathogenesis. J Cell Physiol 2019; 234: 8094-8112.
39. Van Gijsel-Bonnello M, Baranger K, Benech P, Rivera S, Khrestchatisky M, De Reggi M, Gharib B. Metabolic changes and inflammation in cultured astrocytes from the 5xFAD mouse model of Alzheimer's disease: Alleviation by pantethine. PLoS One 2018; 12: e0175369.
40. Wan WB, Chen HX, Li YM. The potential mechanisms of Aβ-receptor for advanced glycation end-products interaction disrupting tight junctions of the blood-brain barrier in Alzheimer's disease. Int J Neurosci 2014; 124: 75-81.
41. Wang L, Tian M, Tang L, Liu B, Yu L. Chronic cerebral hypoperfusion induces ABCA1 and apolipoprotein A I mediated cellular cholesterol efflux by activating LXR/RXR in aging rat brain. Mol Neurodegener 2012; 7: S1-S1.
42. Yan TY, Wang WH, Liu Y, Chen KW, Chen R, Han Y. Rich club disturbances of the human connectome from subjective cognitive decline to Alzheimer's disease. Theranostics 2018; 8: 3237-3255.